

$\rho J/\psi$ Scattering in an Improved Many Body Potential

S. M. Sohail Gilani

Centre For High Energy Physics, Punjab University, Lahore(54590), Pakistan.

M. Imran Jamil

Department of Physics, School of Science,

University of Management and Technology Lahore (54770), Pakistan.

Bilal Masud and Faisal Akram

Centre For High Energy Physics, Punjab University, Lahore(54590), Pakistan.

(Dated: October 14, 2018)

Abstract

We calculate the cross-sections for the processes $\rho J/\psi \rightarrow D^0 \bar{D}^0$, $\rho J/\psi \rightarrow D^0 \bar{D}^{0*}$ ($D^{0*} \bar{D}^0$) and $\rho J/\psi \rightarrow D^{0*} \bar{D}^{0*}$ using a QCD-motivated many-body overlap factor to modify the usual sum of two-body interaction model. The realistic Cornell potential has been used for pairwise interaction in the four quark Hamiltonian and noted to give lesser cross-sections as compared to the quadratic potential. The Resonating group method is employed along with the Born approximation which decouples its integral equations. It is pointed out that the additional QCD effect (a gluonic field overlap factor) result in a significant suppression in the cross sections as compared to the more popular sum of two-body interaction.

PACS numbers:

I. INTRODUCTION

In the quark potential model the gluonic field energy in quantum chromodynamics (QCD) is modelled as the potential energy of the quarks. Its relation with QCD can be seen through the Born-Oppenheimer approach, used for hadronic physics in refs. [1–4]. For one pair of quark and antiquark, Coulombic plus linear or Cornell form [5] for the quark antiquark potential provides a good fit to the total gluonic field energy for the the lattice simulations of the gluonic state Σ_g^+ reported in refs. [6–8] and many earlier ones. For a quark antiquark pair, much use has been made of this potential model to find dynamical implications [9]. Weinstein and Isgur [10, 11] extended this through a sum of such two-body potentials and argued for the $K\bar{K}$ molecule interpretation of the $f_0(975)$ and $a_0(980)$ mesons. They variationally optimized a $q^2\bar{q}^2$ wave function and projected the $q^2\bar{q}^2$ state onto free $q\bar{q}$ wave functions to estimate a relative two meson wave function and an equivalent meson meson potential. T. Barnes and E. Swanson further used the sum of pair-wise approach to calculate [12] $\pi^+\pi^+$, K^+K^+ and $\rho^+\rho^+$ elastic scattering phase shifts and cross sections by using Born-order quark exchange diagrams (in a nonrelativistic potential model) which use Gaussian external meson wave functions. Using the same approach, Barnes et. al. calculated [13] BB intermeson potentials and scattering amplitudes by taking Fourier transform of the Born order T -matrix element of the Hamiltonian between two-mesons scattering states. They compare, in their figures 4 and 5, their nonrelativistic quark model BB potentials with lattice gauge theory (LGT) results of UKQCD Collaboration [14].

The quark exchange (diagrammatic) approach has been used [15, 16] for systems with charm and light quarks, the flavor sectors we address in the present paper. This model was used by Wong et. al. in refs. [17, 18] to calculate the cross sections for the dissociation of J/ψ and ψ' by π and ρ and later the dissociation cross sections for J/ψ , ψ' , χ , Υ and Υ' in collision with π , ρ and K mesons. It is worthwhile judging if this model agrees to the lattice simulations of QCD. Such a comparison was made by UKQCD collaboration and coworkers who noted that the Cornell model extended in this simple way results in binding energy of two quarks and two antiquarks square geometry increasing with each quark separation, whereas the lattice simulations show [19] a decrease. Phenomenologically, the sum of pair wise interactions results in the long range van der Waal's interaction between color singlet mesons that contradicts the relevant experiments. Both of these problems were remedied [20]

by multiplying the off-diagonal elements in the normalization and potential energy matrices, in the relevant color basis, through a space dependent f factor which approaches to 1 in the limit of all the distances approaching to zero and to zero in the limit of large separations.

The actual form of this gluonic field overlap factor f and fit of its parameter(s) to the relevant lattice simulations was improved through refs. [21–24]. Meanwhile, ref. [25] calculated terms in the effective Hamiltonian for quark (and antiquark) kinetic energy operators. This allowed incorporating the quark motion, with the f factor appearing in the off-diagonal elements of the kinetic energy matrices as well. The f factor affects the linear independence of the color configurations. But still a two-states basis was found [23, 24] to be sufficient to well model the relevant computer simulations; we use 2×2 matrices. We have used the simplest (Gaussian) form of f that is used in ref. [24] along with the best fitted value of k_f chosen in it. But, as in refs. [20, 26], we multiply it by the matrix elements of the actual SU(3) color matrices. In these and related calculations [27, 28] for meson-meson cross-sections and bindings, resonating group method (mentioned below in section II) has been employed to use the wave function of a single cluster of a quark antiquark pair. These wave functions are taken to be those of the quadratic confinement; each potential energy is also quadratic in the four papers. In the present paper we fit the parameters of a Gaussian form to the numerically calculated eigenfunctions of the realistic Cornell potential for each cluster, and in the multiquark Hamiltonian we have Cornell potential for each pair-wise interaction. Here we incorporate the spin and flavor dependence and use Born approximation to report the cross sections for the processes $\rho J/\psi \rightarrow D^0 \bar{D}^0$, $\rho J/\psi \rightarrow D^0 \bar{D}^{0*}$ or $D^{0*} \bar{D}^0$, $\rho J/\psi \rightarrow D^{0*} \bar{D}^{0*}$, $D^0 \bar{D}^0 \rightarrow \rho J/\psi$, $D^{0*} \bar{D}^0$ or $D^0 \bar{D}^{0*} \rightarrow \rho J/\psi$ and $D^{0*} \bar{D}^{0*} \rightarrow \rho J/\psi$. The values of T-Matrix elements (phase shifts)[26] are much less than 1 radian which indicates the validity of the Born approximation. It is expected since ref. [12] has in it that “ There is much circumstantial evidence that high-order diagrams are relatively unimportant in hadron spectroscopy and in low energy scattering and decays (excluding the $u\bar{u} \leftrightarrow d\bar{d}$ mixing)” and Born approximation means neglecting these high-order diagrams.

We report a comparison of incorporating the QCD-motivated improved overlap factor f with the more popular sum of two-body approach, along with those of almost a full use of the realistic Cornell potential and of replacing this by a computationally convenient quadratic potential. A quadratic potential is frequently used [29–32] in the hadronic physics including the nucleon-nucleon interaction. In the old Isgur-Karl model, still used in ref. [33], the

leading order quark antiquark interaction is quadratic. Ding Xiaonan in ref. [34] used the quadratic and linear potentials for baryon baryon interaction and got similar phase shifts. Qualitative properties of QCD Benzene found by assuming quadratic confinement in ref. [35] then found the uncertainty in the masses of benzene like structure with three diquark and colour octet states when compared with the linear confinement. Zahra Ghalenovi et. al. in ref. [36] used both linear and quadratic confinement along with Coulomb like term in the potential to calculate mass spectra of heavy and light scalar tetraquarks modelled as bound states of point-like diquark and diantiquark. They also introduced spin spin, spin isospin and isospin isospin interactions during their calculations and found the compatibility with mild influence of the confining potential.

The paper is organized as follows: In Sec. II, we write the total Hamiltonian of the four quark system in the sum of two body approach. And then we write the total state vector of diquark diantiquark system by using the adiabatic approximation. By using the Resonating Group Method we write the resultant integral equations. In Sec. III, we decouple the two coupled equations by using the Born approximation then we solve them. At the end of this section we describe the corresponding changes in the two equations for different studied processes. In Sec. IV we describe the formalism to obtain the cross sections. In Sec. V we describe the phenomenological fitting of the parameters. In Sec. VI we give the obtained cross sections for different processes. Further more we compare the cross sections for two different potentials. We also compare the cross sections for the Gaussian form of f with the simple sum of two body approach as well. A comparison with other works is also given there.

II. THE HAMILTONIAN AND GLUONIC BASIS

In the sum of two body potential model, the total Hamiltonian of the four quarks system is defined as

$$H = \sum_{i=1}^4 \left[m_i + \frac{P_i^2}{2m_i} \right] + \sum_{i<j} (v_{ij} + H_{hyp}^{ij}) \mathbf{F}_i \cdot \mathbf{F}_j, \quad (1)$$

where

$$H_{hyp}^{ij} = -\frac{8\pi\alpha_s}{3m_i m_j} \mathbf{S}_i \cdot \mathbf{S}_j \delta(r_{ij}). \quad (2)$$

For the i th particle, m_i is constituent quark mass, \mathbf{S}_i is the set of spin matrices, and \mathbf{F}_i is the set of $SU(3)_c$ matrices. The components of \mathbf{F} are $\frac{\lambda_a}{2}$ for a quark and $-\frac{\lambda_a^*}{2}$ for an anti quark, with $a = 1, 2, 3, \dots, 8$. The v_{ij} is inter-quark Cornell potential, which is

$$v(\mathbf{r}_{ij}) = v_{ij} = \frac{\alpha_s}{r_{ij}} - \frac{3}{4}b r_{ij} + c \quad \text{with } i, j = 1, 2, \bar{3}, \bar{4}. \quad (3)$$

Here b is string tension, α_s is strong coupling constant and c is the self energy constant. We incorporate the energy and hence flavor dependence of the strong coupling and self energy constant by taking their values to be α_{s1} and c_1 for the mesons having quarks content $u\bar{c}$, and α_{s2} , c_2 and α_{s3} , c_3 for the $u\bar{u}$ and $c\bar{c}$ clusters respectively. The phenomenological fitting of these parameters is given in Sec. V. In the same way, where we use for a comparison the quadratic potential

$$v(\mathbf{r}_{ij}) = v_{ij} = Cr_{ij}^2 + \bar{C} \quad (4)$$

the three C 's along with \bar{C} are phenomenologically fitted as in Sec. V.

The total state vector of our diquark diantiquark system can be written as

$$|\psi(\mathbf{r}_1, \mathbf{r}_2, \mathbf{r}_3, \mathbf{r}_4; g)\rangle = \sum_{k=1}^2 |k\rangle_g |k\rangle_s |k\rangle_f |\psi(\mathbf{r}_1, \mathbf{r}_2, \mathbf{r}_3, \mathbf{r}_4)\rangle. \quad (5)$$

We have neglected the third topology of Fig. 1 because the lattice energies in Table IV of Ref. [37] are essentially unaffected by this truncation. $\{|k\rangle_g\}$ is the gluonic basis which reduces to color basis $\{|1_{1\bar{3}}1_{2\bar{4}}\rangle, |1_{1\bar{4}}1_{2\bar{3}}\rangle\}$ in the weak coupling limit. The spin basis is composed of

$$|1\rangle_s = \begin{cases} |P_{1\bar{3}}P_{2\bar{4}}\rangle_0 & \text{for } D^0\bar{D}^0 \\ |V_{1\bar{3}}V_{2\bar{4}}\rangle_{0,1 \text{ or } 2} & \text{for } D^{0*}\bar{D}^{0*} \\ |P_{1\bar{3}}V_{2\bar{4}}\rangle_1 & \text{for } D^0\bar{D}^{0*} \end{cases}, \quad (6)$$

$$|2\rangle_s = |V_{1\bar{4}}V_{2\bar{3}}\rangle_{0,1 \text{ or } 2} \quad \text{for } \rho J\psi. \quad (7)$$

These spin states are explicitly defined with their overlaps and $\mathbf{S.S}$ matrix elements in the Appendix A. The flavor contents of first and 2nd channel are

$$|1\rangle_f = |u\bar{c}\rangle_{1\bar{3}}|c\bar{u}\rangle_{2\bar{4}}, \quad (8)$$

$$|2\rangle_f = \frac{1}{\sqrt{2}}|u\bar{u} - d\bar{d}\rangle_{1\bar{4}}|c\bar{c}\rangle_{2\bar{3}}, \quad (9)$$

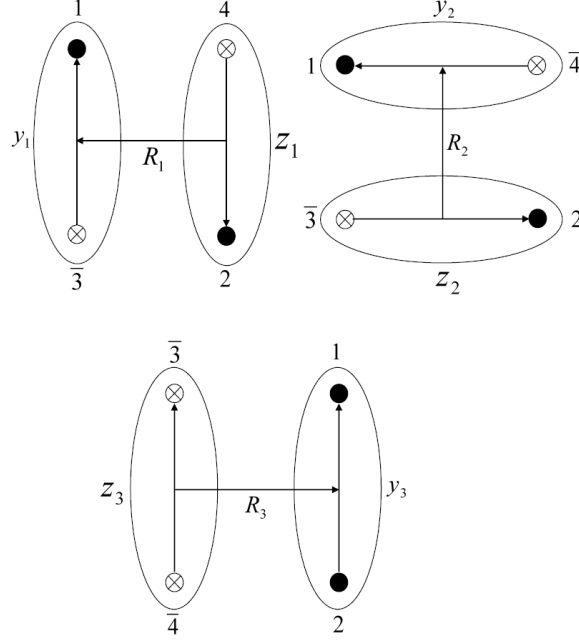


FIG. 1: Different topologies of diquark and diantiquark system.

which gives

$${}_f\langle 1|2\rangle_f = {}_f\langle 2|1\rangle_f = \frac{1}{\sqrt{2}}. \quad (10)$$

The four 3-vectors $\mathbf{r}_1, \mathbf{r}_2, \mathbf{r}_3$ and \mathbf{r}_4 can be replaced by their linear combinations as \mathbf{R}_c (center of mass) along with $\mathbf{R}_k, \mathbf{y}_k$ and \mathbf{z}_k shown in Fig. 1. This means

$$\mathbf{R}_1 = \frac{(\mathbf{r}_1 - \mathbf{r}_4) + r_c(\mathbf{r}_3 - \mathbf{r}_2)}{1 + r_c}, \quad (11)$$

where $r_c = \frac{m_c}{m_u}$. \mathbf{R}_2 and \mathbf{R}_3 are similarly defined. As in the resonating group method, we factorize the dependence on the three relative vectors as a product of the inter-cluster (\mathbf{R}_k) dependence and the intra-clusters (\mathbf{y}_k and \mathbf{z}_k) dependence. This makes the total state vector as

$$|\psi(\mathbf{r}_1, \mathbf{r}_2, \mathbf{r}_3, \mathbf{r}_4; g)\rangle = \sum_{k=1}^2 |k\rangle_g |k\rangle_s |k\rangle_f \psi_c(\mathbf{R}_c) \chi_k(\mathbf{R}_k) \xi_k(\mathbf{y}_k) \zeta_k(\mathbf{z}_k). \quad (12)$$

$\xi_k(\mathbf{y}_k)$ and $\zeta_k(\mathbf{z}_k)$ are intra-cluster wave functions which we take to be in Gaussian form as following

$$\xi_k(\mathbf{y}_k) = \frac{1}{(2\pi d_{k1}^2)^{3/4}} \exp\left(\frac{-\mathbf{y}_k^2}{4d_{k1}^2}\right), \quad (13)$$

$$\zeta_k(\mathbf{z}_k) = \frac{1}{(2\pi d_{k2}^2)^{3/4}} \exp\left(\frac{-\mathbf{z}_k^2}{4d_{k2}^2}\right), \quad (14)$$

where d_{k1} and d_{k2} are corresponding mesonic sizes.

Substituting Eq. (12) in

$$\langle \delta\Psi | H - E | \Psi \rangle = 0 \quad (15)$$

and taking linearly independent variations only in χ_k factor, along with performing the trivial \mathbf{R}_c integration using, say, a box normalization, we get

$$\sum_{l=1}^2 \int d^3\mathbf{y}_k d^3\mathbf{z}_k \xi_k(\mathbf{y}_k) \zeta_k(\mathbf{z}_k) {}_f\langle k | {}_s\langle k | {}_g\langle k | H - E | l \rangle_g | l \rangle_s | l \rangle_f \chi_l(\mathbf{R}_l) \xi_l(\mathbf{y}_l) \zeta_l(\mathbf{z}_l) = 0, \quad (16)$$

which defines two integral equations for $k=1$ and 2 . The matrix elements of potential energy part of the Hamiltonian in our spin basis are given by

$${}_s\langle k | V(f) | l \rangle_s = \sum_{i < j} \mathbf{F}_i \cdot \mathbf{F}_j(f) (V_{ij})_{k,l}, \quad (17)$$

with

$$(V_{ij})_{k,l} = v_{ij} {}_s\langle k | l \rangle_s - \frac{8\pi\alpha_s}{3m_i m_j} \delta(r_{ij}) {}_s\langle k | \mathbf{S}_i \cdot \mathbf{S}_j | l \rangle_s. \quad (18)$$

Now using the matrix elements of $\mathbf{F}_i \cdot \mathbf{F}_j$ operator in the colour basis [10] in the potential energy matrix, defined in Eq. (17) above, in gluonic basis modified by f model is given by

$$V(f) = \begin{pmatrix} -\frac{4}{3}(V_{1\bar{3}} + V_{2\bar{4}})_{1,1} & \frac{4f}{9}(V_{12} + V_{\bar{3}\bar{4}} - V_{1\bar{3}} - V_{2\bar{4}} - V_{1\bar{4}} - V_{2\bar{3}})_{1,2} \\ \frac{4f}{9}(V_{12} + V_{\bar{3}\bar{4}} - V_{1\bar{3}} - V_{2\bar{4}} - V_{1\bar{4}} - V_{2\bar{3}})_{2,1} & -\frac{4}{3}(V_{1\bar{3}} + V_{2\bar{4}})_{2,2} \end{pmatrix}. \quad (19)$$

Here, f , is defined as [24]

$$f = \exp(-bk_f \sum_{i < j} r_{ij}^2), \quad (20)$$

where k_f is a parameter fitted to minimize the model and simulation binding energies. The color basis is non-orthogonal. Thus there is a non-trivial overlap matrix which is modified by the f -model to become

$$N(f) \equiv \{{}_g\langle k | l \rangle_g\} = \begin{pmatrix} 1 & \frac{f}{3} \\ \frac{f}{3} & 1 \end{pmatrix}. \quad (21)$$

The k, l matrix element of the kinetic energy matrix (in a Hermitian form) in the gluonic basis is

$${}_g\langle k | K | l \rangle_g = N(f)_{k,l}^{1/2} \left(\sum_i -\frac{\nabla_i^2}{2m_i} \right) N(f)_{k,l}^{1/2}. \quad (22)$$

III. WRITING THE COUPLED EQUATIONS

The total spin for each of $\rho J/\Psi \rightarrow D^0 \bar{D}^0$ and $D^0 \bar{D}^0 \rightarrow \rho J/\Psi$ is zero. For the first channel we take $k = 1$ in Eq. (16). Our Hamiltonian is identity in the flavor space, so we use flavor overlaps from Eq. (10). The spin overlaps and $\mathbf{S} \cdot \mathbf{S}$ matrix elements in spin basis are given in Appendix A. We insert the elements of P.E., Normalization and K.E Matrices from Eqs. (19, 21 and 22) in Eq. (16) and use Born approximation i.e. non-interacting $\chi_1(\mathbf{R}_1) = \sqrt{2/\pi} e^{i\mathbf{P}_1 \cdot \mathbf{R}_1}$ to decouple the two coupled equations (see Eq. (16)). Performing the Fourier transform with respect to \mathbf{R}_1 we get

$$(k_1 + k_2 \mathbf{P}_1^2 - E + 2m_u(1 + r_c))\chi_1(\mathbf{P}_1) = h_{12}, \quad \text{where} \quad (23)$$

$$h_{12} = \frac{1}{(2\pi)^{\frac{3}{2}}} \frac{1}{\sqrt{2}} \int d^3\mathbf{y}_1 d^3\mathbf{z}_1 d^3\mathbf{R}_1 \xi_1(\mathbf{y}_1) \zeta_1(\mathbf{z}_1) \sqrt{f} \left\{ -\frac{4}{9}(V_c - V_{hyp}) \sqrt{f} e^{i\mathbf{P}_2 \cdot \mathbf{R}_2} \xi_2(\mathbf{y}_2) \right. \\ \left. \zeta_2(\mathbf{z}_2) + \mathcal{K}_{12} - \mathcal{N}_{12} \right\} \sqrt{\frac{2}{\pi}} e^{i\mathbf{P}_1 \cdot \mathbf{R}_1}. \quad (24)$$

In Eq. (24) V_c , V_{hyp} , \mathcal{K}_{12} and \mathcal{N}_{12} are defined as

$$V_c = \frac{-\sqrt{3}}{2} \left\{ \alpha_{s1} \left(\frac{1}{y_3} + \frac{1}{z_3} - \frac{1}{y_1} - \frac{1}{z_1} \right) - \frac{\alpha_{s2}}{y_2} - \frac{\alpha_{s3}}{z_2} \right. \\ \left. - \frac{3}{4} b_s (y_3 + z_3 - y_1 - z_1 - y_2 - z_2) - c_2 - c_3 \right\}. \quad (25)$$

$$V_{hyp} = \frac{\sigma^3}{\sqrt{3\pi}} \left\{ \alpha_{s1} \left(\frac{e^{-\sigma^2 \mathbf{y}_3^2}}{m_u m_c} + \frac{e^{-\sigma^2 \mathbf{z}_3^2}}{m_c m_u} - \frac{3e^{-\sigma^2 \mathbf{y}_1^2}}{m_u m_c} - \frac{3e^{-\sigma^2 \mathbf{z}_1^2}}{m_c m_u} \right) + \frac{\alpha_{s2} e^{-\sigma^2 \mathbf{y}_2^2}}{m_u m_u} + \frac{\alpha_{s3} e^{-\sigma^2 \mathbf{z}_2^2}}{m_c m_c} \right\}. \quad (26)$$

$$\mathcal{K}_{12} = \frac{1}{2\sqrt{3}} \left(-\frac{1}{2m_u} \right) \left[\xi_2(\mathbf{y}_2) \zeta_2(\mathbf{z}_2) f_2 \nabla_{\mathbf{R}_2}^2 (\sqrt{f} e^{i\mathbf{P}_2 \cdot \mathbf{R}_2}) + e^{i\mathbf{P}_2 \cdot \mathbf{R}_2} \zeta_2(\mathbf{z}_2) g_2 \nabla_{\mathbf{y}_2}^2 (\sqrt{f} \xi_2(\mathbf{y}_2)) \right. \\ \left. + e^{i\mathbf{P}_2 \cdot \mathbf{R}_2} \xi_2(\mathbf{y}_2) h_2 \nabla_{\mathbf{z}_2}^2 (\sqrt{f} \zeta_2(\mathbf{z}_2)) \right], \quad (27)$$

where $f_2 = \frac{1}{2}(\frac{1+r_c}{r_c})$, $g_2 = 2$, and $h_2 = \frac{2}{r_c}$.

$$\mathcal{N}_{12} = (E - 2m_u(1 + r_c)) \left(\frac{1}{2\sqrt{3}} \right) \sqrt{f} e^{i\mathbf{P}_2 \cdot \mathbf{R}_2} \xi_2(\mathbf{y}_2) \zeta_2(\mathbf{z}_2). \quad (28)$$

We chose z -axis along \mathbf{P}_1 and x -axis in the plane containing \mathbf{P}_1 and \mathbf{P}_2 . Naming the angle between \mathbf{P}_1 and \mathbf{P}_2 as θ , we get $P_{2x} = P_2 \sin \theta$, $P_{2z} = P_2 \cos \theta$, $P_{2y} = 0$, along with $P_{1x} = P_{1y} = 0$, $P_{1z} = P_1$.

Similarly, for the second channel, we take $k = 2$ in Eq. (16) and apply the same procedure as for Eq.(23) to get

$$(k_3 + k_4 \mathbf{P}_2^2 - E + 2m_u(1 + r_c))\chi_2(\mathbf{P}_2) = h_{21}, \quad \text{where} \quad (29)$$

$$h_{21} = \frac{1}{(2\pi)^{\frac{3}{2}}} \frac{1}{\sqrt{2}} \int d^3\mathbf{y}_2 d^3\mathbf{z}_2 d^3\mathbf{R}_2 \xi_2(\mathbf{y}_2) \zeta_2(\mathbf{z}_2) \sqrt{f} \left\{ -\frac{4}{9}(V_c - V_{hyp}) \sqrt{f} e^{i\mathbf{P}_1 \cdot \mathbf{R}_1} \right. \\ \left. \xi_1(\mathbf{y}_1) \zeta_1(\mathbf{z}_1) + \mathcal{K}_{21} - \mathcal{N}_{21} \right\} \sqrt{\frac{2}{\pi}} e^{i\mathbf{P}_2 \cdot \mathbf{R}_2}. \quad (30)$$

V_c and V_{hyp} are same as in Eq. (23). \mathcal{K}_{21} and \mathcal{N}_{21} are defined as

$$\mathcal{K}_{21} = \frac{1}{2\sqrt{3}} \left(-\frac{1}{2m_u} \right) \sqrt{f} [\xi_1(\mathbf{y}_1) \zeta_1(\mathbf{z}_1) f_1 \nabla_{\mathbf{R}_1}^2 (\sqrt{f} e^{i\mathbf{P}_1 \cdot \mathbf{R}_1}) + e^{i\mathbf{P}_1 \cdot \mathbf{R}_1} \zeta_1(\mathbf{z}_1) g_1 \\ \nabla_{\mathbf{y}_1}^2 (\sqrt{f} \xi_1(\mathbf{y}_1)) + e^{i\mathbf{P}_1 \cdot \mathbf{R}_1} \xi_1(\mathbf{y}_1) h_1 \nabla_{\mathbf{z}_1}^2 (\sqrt{f} \zeta_1(\mathbf{z}_1))], \quad (31)$$

where $f_1 = \frac{2}{1+r_c}$, $g_1 = \frac{1+r_c}{r_c}$ and $h_1 = \frac{1+r_c}{r_c}$.

$$\mathcal{N}_{21} = (E - 2m_u(1 + r_c)) \frac{1}{2\sqrt{3}} \sqrt{f} e^{i\mathbf{P}_1 \cdot \mathbf{R}_1} \xi_1(\mathbf{y}_1) \zeta_1(\mathbf{z}_1). \quad (32)$$

Above is for the processes $\rho J/\Psi \rightarrow D^0 \bar{D}^0$ and $D^0 \bar{D}^0 \rightarrow \rho J/\Psi$. Due to different spin states the hyperfine term for the process $\rho J/\psi \rightarrow D^0 \bar{D}^{0*}$ or $D^0 \bar{D}^{0*} \rightarrow \rho J/\psi$ is given instead by

$$V_{hyp} = -\sqrt{\frac{2}{3}} \frac{\sigma^3}{\sqrt{3\pi}} \left\{ \alpha_{s1} \left(\frac{e^{-\sigma^2 \mathbf{y}_3^2}}{m_u m_c} + \frac{e^{-\sigma^2 \mathbf{z}_3^2}}{m_c m_u} - \frac{3e^{-\sigma^2 \mathbf{y}_1^2}}{m_u m_c} + \frac{e^{-\sigma^2 \mathbf{z}_1^2}}{m_c m_u} \right) + \frac{\alpha_{s2} e^{-\sigma^2 \mathbf{y}_2^2}}{m_u m_u} + \frac{\alpha_{s3} e^{-\sigma^2 \mathbf{z}_2^2}}{m_c m_c} \right\}, \quad (33)$$

and all the remaining terms of Eqs. (24 and 30) are multiplied by a factor $-\sqrt{2/3}$, because the corresponding spin overlap of the above mentioned processes is $1/\sqrt{2}$.

For the process $\rho J/\psi \rightarrow D^{0*} \bar{D}^{0*}$ or $D^{0*} \bar{D}^{0*} \rightarrow \rho J/\psi$ the hyperfine term differs with the total spin. For total spin zero this becomes

$$V_{hyp} = \frac{1}{\sqrt{3}} \frac{\sigma^3}{\sqrt{3\pi}} \left\{ \alpha_{s1} \left(\frac{5e^{-\sigma^2 \mathbf{y}_3^2}}{m_u m_c} + \frac{5e^{-\sigma^2 \mathbf{z}_3^2}}{m_c m_u} + \frac{e^{-\sigma^2 \mathbf{y}_1^2}}{m_u m_c} + \frac{e^{-\sigma^2 \mathbf{z}_1^2}}{m_c m_u} \right) + \frac{\alpha_{s2} e^{-\sigma^2 \mathbf{y}_2^2}}{m_u m_u} + \frac{\alpha_{s3} e^{-\sigma^2 \mathbf{z}_2^2}}{m_c m_c} \right\}, \quad (34)$$

and all the remaining terms of Eqs. (24 and 30) are multiplied by a factor $1/\sqrt{3}$, because the corresponding spin overlap of the above mentioned processes is $-1/2$. For total spin 2 the hyperfine term becomes

$$V_{hyp} = \frac{2}{\sqrt{3}} \frac{\sigma^3}{\sqrt{3\pi}} \left\{ \alpha_{s1} \left(\frac{e^{-\sigma^2 \mathbf{y}_3^2}}{m_u m_c} + \frac{e^{-\sigma^2 \mathbf{z}_3^2}}{m_c m_u} - \frac{e^{-\sigma^2 \mathbf{y}_1^2}}{m_u m_c} - \frac{e^{-\sigma^2 \mathbf{z}_1^2}}{m_c m_u} \right) - \frac{\alpha_{s2} e^{-\sigma^2 \mathbf{y}_2^2}}{m_u m_u} - \frac{\alpha_{s3} e^{-\sigma^2 \mathbf{z}_2^2}}{m_c m_c} \right\}, \quad (35)$$

and all the remaining terms of Eqs. (24 and 30) are multiplied by a factor $-2/\sqrt{3}$, because the corresponding spin overlap of the above mentioned processes is 1.

When we use quadratic potential then only potential part of the integral Eqs. (23 and 29) is changed. That is V_c is replaced by V_q , where

$$V_q = \frac{-\sqrt{3}}{2} \left\{ C_2 \left(\mathbf{y}_3^2 + \mathbf{z}_3^2 - \mathbf{y}_1^2 - \mathbf{z}_1^2 \right) - C_3 \mathbf{y}_2^2 - C_1 \mathbf{z}_2^2 - 2\bar{C} \right\}. \quad (36)$$

Here, C_1 is a constant of inter-quark potential (see Eq. 4) of $c\bar{c}$ mesons, C_2 is constant for $c\bar{u}$ or $u\bar{c}$ mesons and C_3 is constant for $u\bar{u}$ mesons. When we use quadratic potential in the coupled equations (16), the spin averaging is used to fit the parameters given in Sec. V and hence the hyperfine term is neglected.

IV. FINDING THE CROSS-SECTIONS

The T matrix elements can be read off from Eqs. (23) and (29). These would be proportional to the coefficients (h_{12} and h_{21}) of the non relativistic Green operators $-1/\Delta_1(P_1)$ and $-1/\Delta_2(P_2)$, where

$$\Delta_1(P_1) = (k_1 + k_2 \mathbf{P}_1^2 - E + 2m_u(1 + r_c)) \quad \text{and} \quad (37)$$

$$\Delta_2(P_2) = (k_3 + k_4 \mathbf{P}_2^2 - E + 2m_u(1 + r_c)). \quad (38)$$

That is, [27]

$$T_{12} = 2\mu_{12} \frac{\pi}{2} P_2 \sqrt{\frac{v_1}{v_2}} h_{12} \quad (39)$$

$$T_{21} = 2\mu_{34} \frac{\pi}{2} P_1 \sqrt{\frac{v_2}{v_1}} h_{21}, \quad (40)$$

where $i, j = 1, 2$ and P_j are relative momenta of two clusters for channel 1 and 2 defined as

$$P_1 = \sqrt{2\mu_{12}(E - M_1 - M_2)} \quad \text{and} \quad (41)$$

$$P_2 = \sqrt{2\mu_{34}(E - M_3 - M_4)}. \quad (42)$$

Here $M_i, i = 1, 2, 3, 4$ are corresponding meson masses and μ_{ij} are reduce masses of corresponding mesons, $v_1 = P_1/\mu_{12}$, $v_2 = P_2/\mu_{34}$. Finally we get the spin averaged cross-sections by using the following equation [38]

$$\sigma_{ij} = \frac{4\pi}{P_j^2} \sum_J \frac{2J+1}{(2s_1+1)(2s_2+1)} |T_{ij}|^2, \quad (43)$$

where J is the total spin of the two outgoing mesons and s_1 and s_2 are the spins of the two incoming mesons.

V. FITTING THE PARAMETERS

The parameters for Cornell Potential i.e α_s and c are fitted by finding minimum Chi square between the masses taken from PDG and the mass spectrum generated using Cornell model in the quark potential model for the mesons $\rho_0, b_1, a, D^0, D^{0*}, D_1, D_2^*, \eta_c, J/\psi, h_c$ and χ_c . The fitted parameters are $\alpha_{s1} = 0.38$, $\alpha_{s2} = \alpha_{s3} = 0.5$, $c_1 = 0.732$, $c_2 = 0.692$, and $c_3 = 0.612$. The values $m_u = 0.345$, $m_c = 1.931$, $k_f = 0.075$, $b_s = 0.18$, and $\sigma = 0.897$ are taken from Refs. [17, 18, 24]. In quadratic potential ω , m_u and m_c are fitted by minimizing the chi-square $\chi^2 = \sum_i ((E_i - \tilde{E}_i)/\tilde{E}_i)^2$, where \tilde{E}_i are the spin averaged experimental masses [39] and E_i are the masses obtained by $E_i = (\omega/2)(4n+2l+3) + m_0$ [40], that is 3-d S.H.O. energy and the rest mass energy. Here i labels the different mesons. We have used the following spectrum to fit the parameters $\eta_c, J/\psi, \chi_{c0}, \chi_{c1}, \chi_{c2}, D^0, D^{0*}, D_1, D_2, \rho, \omega, a_1, a_2, b_1, \pi(1300), \rho_3$ and π_2 . After getting ω the constants and mesons sizes are obtained by using $C = -(3/16)(2\mu\omega^2)$ and $d = \sqrt{1/2\mu\omega}$ [20, 27]. Hence the fitted parameters are $m_u = 0.1065$, $m_c = 1.2877$, $C_1 = -0.0273$, $C_2 = -0.00615$, $C_3 = -0.002995$ and $\bar{C} = 0$. The resulting meson sizes for both quadratic and Cornell potential are given in Table I, along with the meson masses used in the fitting taken from PDG.

		Cornell potential	Quadratic Potential
Meson	Mass(GeV)	d(GeV ⁻¹)	d(GeV ⁻¹)
ρ	0.77549	2.3827	4.9241
D^0/\bar{D}^0	1.86483	1.6543	3.5288
D^{0*}/\bar{D}^{0*}	2.00698	1.9238	3.5288
J/ψ	3.096916	0.9947	1.5199

TABLE I: Mesons Masses and their corresponding sizes for Cornell and quadratic Potentials.

VI. RESULTS AND CONCLUSIONS

The values of cross sections of $\rho J/\psi \rightarrow D^0 \bar{D}^0$, $\rho J/\psi \rightarrow D^0 \bar{D}^{0*}$ ($D^{0*} \bar{D}^0$), $\rho J/\psi \rightarrow D^{0*} \bar{D}^{0*}$ and corresponding inverse processes by using Cornell as well as quadratic potentials are given in figures (2) to (9). These cross sections are first obtained by using $f = 1$ and latter by using

Gaussian form of f . In these figures $T_c = E_c - m_{D^{0*}} - m_{\bar{D}^{0*}}$ for the processes $\rho J/\psi \rightarrow D^{0*} \bar{D}^{0*}$ and $D^{0*} \bar{D}^{0*} \rightarrow \rho J/\psi$ and $T_c = E_c - m_\rho - m_{J/\psi}$ for remaining four processes, where E_c is total centre of mass energy. The processes $\rho J/\psi \rightarrow D^0 \bar{D}^0$, $\rho J/\psi \rightarrow D^0 \bar{D}^{0*}/D^{0*} \bar{D}^0$ and $D^{0*} \bar{D}^{0*} \rightarrow \rho J/\psi$ are exothermic where as all the remaining processes are endothermic. In all plots we can observe that the cross sections obtained for the quadratic potential have different shapes as compared to the Cornell potential. All the reactions show larger cross sections for the quadratic potential when compared with the Cornell potential.

There is a significant suppression in the cross sections obtained when factor f is introduced as compared to the cross sections obtained from simple sum of two body approach. We can observe this suppression easily in all endothermic reactions where the peak of these cross sections is decreased by factor of 14 to 20 after including the factor f . For the process $\rho J/\psi \rightarrow D^0 \bar{D}^{0*}$ or $D^{0*} \bar{D}^0$ there is 18 times suppression in the cross sections for the Cornell potential after including f where as for quadratic potential this suppression is 14 times. After including f the suppressions in the cross sections for the process $D^0 \bar{D}^0 \rightarrow \rho J/\psi$ are nearly 16 and 7 times for the Cornell and the quadratic potentials respectively and for the process $D^0 \bar{D}^{0*}$ or $D^{0*} \bar{D}^0 \rightarrow \rho J/\psi$ these suppressions are 20 and 18 times for the Cornell and the quadratic potentials respectively. It is noted that the Gaussian form of f factor produces larger suppression in case of Cornell as compared to quadratic potential. To elucidate this effect we produce the plots of potential energy and remaining terms which include kinetic energy and constant terms verses T_c for a specific process $\rho J/\psi \rightarrow D^0 \bar{D}^0$. The resultant values of cross sections depend on delicate cancelation in these terms. The Fig. 10 shows that in case of Cornell potential these terms are modified by the f factor in such a way that cancelation is higher as compared to quadratic potential for which the similar plot is given in Fig. 11.

Kevin L. Haglin and Charles Gale in ref. [41] used chiral Lagrangian approach for heavy light mesons to study the cross sections of different J/ψ reactions. The peak of the cross section for the process $\rho J/\psi \rightarrow D^* \bar{D}^*$ near threshold is 5 mb in figure (3) of ref. [41] which is comparable with the dashed curve of our figure (3) where we are using quadratic potential and $f=1$. In figure (4) Haglin et. al. also reported the cross sections for the process $\rho J/\psi \rightarrow D \bar{D}$. Here cross section is maximum near threshold and decreases to zero at total centre of mass energy 4.2 GeV. These cross sections are comparable with the solid curve of our figure (5) where we are using quadratic potential and Gaussian form of f . The

other processes reported in our paper are not calculated by Haglin et. al.

Ziwei Lin and C. M. Ko in ref. [42] used an effective hadronic Lagrangian to obtain the cross sections for different J/ψ reactions. In figure (4) of this reference, Ziwei et. al. reported the cross sections for the process $\rho J/\psi \rightarrow D^* \bar{D}^*$ and $\rho J/\psi \rightarrow D \bar{D}$. In this figure the peak of the cross section for the process $\rho J/\psi \rightarrow D^* \bar{D}^*$ is 9 mb near threshold without form factor which is nearly double than that of the cross section obtained in our figure (3) when we are using quadratic potential with $f=1$. But when they introduced a form factor then the peak of the cross section becomes approximately 5 mb which agrees with our result for quadratic potential as in figure (3). Yongseok Oh, Taesoo Song, and Su Houng Lee in ref. [43] also used effective Lagrangian for the J/ψ absorption by π and ρ mesons. In figure (6) Yongseok et. al. reported the cross sections for the processes $\rho J/\psi \rightarrow D \bar{D}$, $\rho J/\psi \rightarrow D^* \bar{D} (D \bar{D}^*)$ and $\rho J/\psi \rightarrow D^* \bar{D}^*$. The shape of their plots is different with our plots except for the process $\rho J/\psi \rightarrow D \bar{D}$ which damps at total centre of mass energy 4.08 GeV corresponding to $T_c = 0.2$ GeV in agreement with our result obtained using the Cornell potential. The effective Lagrangian approach used in above mentioned refs. [42, 43] is somewhat unrealistic as it is based on using SU(4) flavour symmetry which is badly broken in QCD due to large charm quark mass as compared to light quarks.

In ref. [17] Cheuk-Yin Wong, E. S. Swanson and T. Barnes evaluated the cross sections for different processes using the quark interchange model of Barnes and Swanson [12]. In figure (3) of this ref. [17] Wong et. al. reported the cross sections for the processes $\rho J/\psi \rightarrow D \bar{D}$, $\rho J/\psi \rightarrow D^* \bar{D}$ or $D \bar{D}^*$ and $\rho J/\psi \rightarrow D^* \bar{D}^*$. Their cross section for the process $\rho J/\psi \rightarrow D \bar{D}$ damped at T_c nearly equal to 0.5 GeV whereas in our figures (2) and (4) it is damped at $T_c = 0.2$ GeV for Cornell Potential with $f=1$ and in our figure (5) the cross section is damped for the same process at T_c nearly equal to 0.5 GeV when we use quadratic potential along with Gaussian form of f . However this damping is at $T_c = 0.2$ GeV in their later work [18]. In these papers Wong et. al. reported the cross sections for the process $\rho J/\psi \rightarrow D^* \bar{D}^*$ with total spin 0, 1 and 2 separately whereas we are reporting spin averaged cross sections. Wong et. al. in their approach used the Cornell potential but not included f . We are reporting our cross sections after improving the potential by including f . In figures (5) and (6) of ref. [28] the cross sections are reported for the process $\rho J/\psi \rightarrow D^0 \bar{D}^{0*}$ and $D^0 \bar{D}^{0*} \rightarrow \rho J/\psi$. In this reference only quadratic potential is used with $f = 1$ and Gaussian form of f . In our current work we are using broader spectrum to fit the parameters which cause a little

change in these cross sections with this given reference. Moreover, in our recent work we are replacing quadratic potential by more realistic Cornell potential while keep using $f=1$ and Gaussian form of f as well.

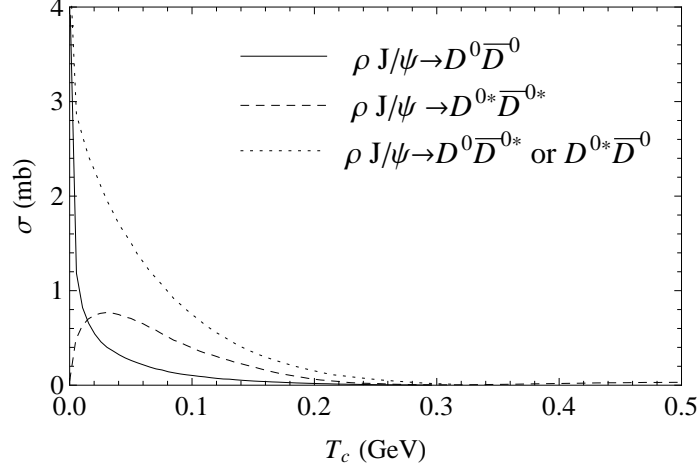


FIG. 2: Graph between Cross sections and T_c for Cornell potential with $f = 1$.

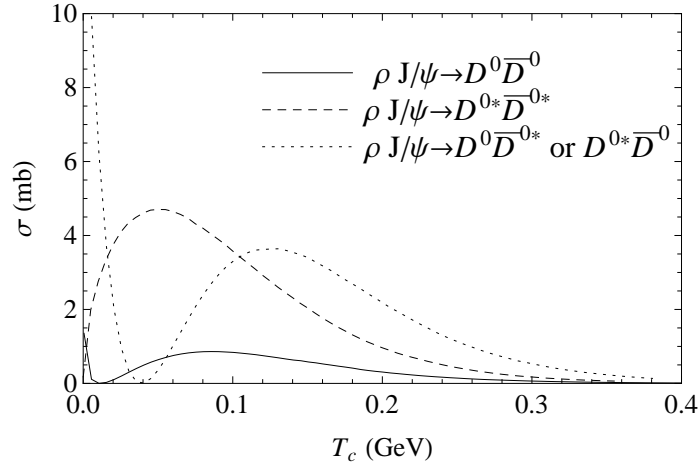


FIG. 3: Graph between Cross sections and T_c for Quadratic potential with $f = 1$.

-
- [1] K. J. Juge, J. Kuti, C. J. Morningstar, Phys. Rev. Lett. **82**, 4400 (1999).
 - [2] Nosheen Akbar, Bilal Masud and Saba Noor, Eur. Phys. J. A**47**, 124 (2011).
 - [3] A. Sultan, N. Akbar, B. Masud, F. Akram, Phys. Rev. D **90**, 054001 (2014).

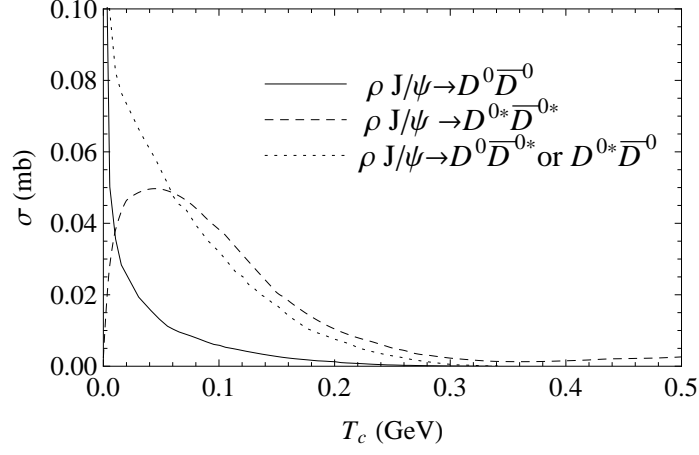


FIG. 4: Graph between Cross sections and T_c for Cornell potential with Gaussian form of f .

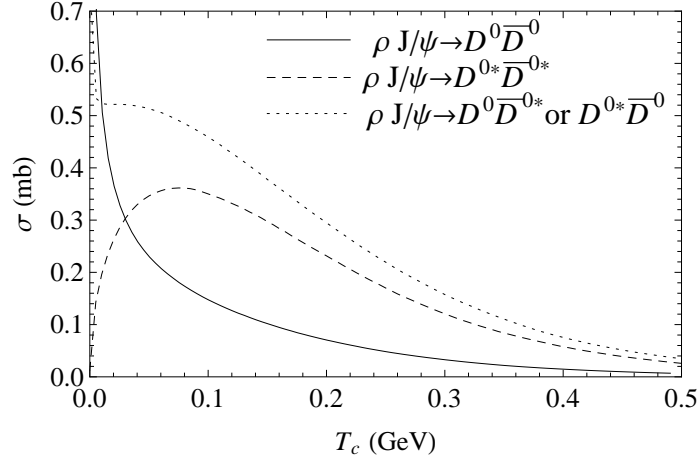


FIG. 5: Graph between Cross sections and T_c for Quadratic potential with Gaussian form of f .

- [4] E. Braaten, C. Langmack, D. H. Smith, Phys. Rev. D **90**, 014044 (2014).
- [5] E. Eichten, K. Gottfried, T. Kinoshita, K. D. Lane and T. -M. Yan, Phys. Rev. D **17**, 3090 (1978), Phys. Rev. D **21(E)**, 313 (1980).
- [6] K. J. Juge, J. Kuti and C. Morningstar, AIP Conf. Proc. **688**, 193 (2003).
- [7] Bali G S et al. , Phys. Rev **D62**, 054503 (2000).
Bali G S, Phys. Rep.**343**, 1 (2001).
- [8] Alexandrou C, de Forcrand P and John O, Nucl. Phys. **B119**, 667 (2003).
- [9] Stephen Godfrey and Nathan Isgur, Phys. Rev. **D32** 1 (1985).
- [10] John Weinstein and Nathan isgur, Phys. Rev. **D41**, 7 (1990).
- [11] J. Weinstein, N. Isgur, Phys. Rev. **D27**, 588 (1983).

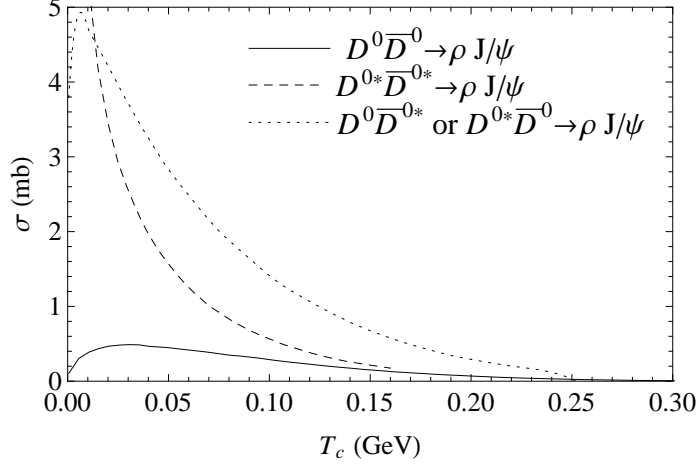


FIG. 6: Graph between Cross sections and T_c for Cornell potential with $f = 1$ (reverse processes).

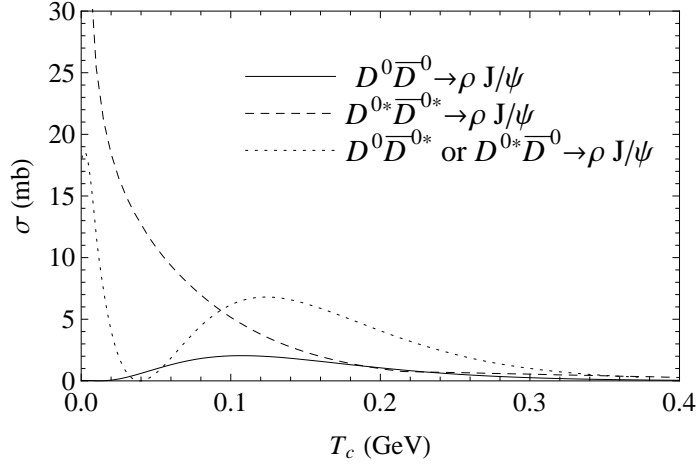


FIG. 7: Graph between Cross sections and T_c for Quadratic potential with $f = 1$ (reverse processes).

- [12] T. Barnes and E. S. Swanson, Phys. Rev. **D46**, 131 (1992).
- [13] T. Barnes, N. Black, D. J. Dean and E. S. Swanson, Phys. Rev. **C60**, 045202 (1999).
- [14] C. Michael, and P. Pennanen, Phys. Rev. **D60**, 054012 (1999).
- [15] K. Martins, D. Blaschke, and E. Quack, Phys. Rev. **C51**, 2723 (1995).
- [16] T. Barnes, E. S. Swanson, C. -Y. Wong and X. -M. Xu, Phys. Rev. **C68**, 014903 (2003).
- [17] Cheuk-Yin Wong, E. S. Swanson and T. Barnes, Phys. Rev. **C62**, 045201 (2000).
- [18] Cheuk-Yin Wong, E. S. Swanson and T. Barnes, Phys. Rev. **C65**, 014903 (2001).
- [19] A. M. Green, C. Michael and J. E. Paton, Nucl. Phys. **A554**, 701 (1993).
- [20] B. Masud, J. Paton, A. M. Green and G. Q. Liu, Nucl. Phys. **A 528**, 477 (1991).
- [21] S. Furui, A. M. Green, B. Masud, Nucl. Phys. **A582**, 682 (1995).

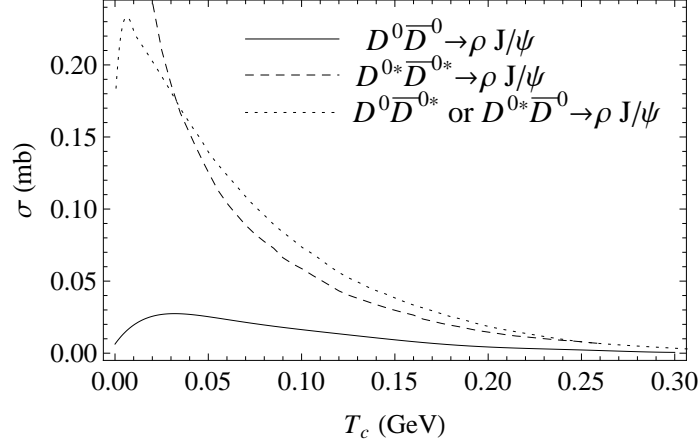


FIG. 8: Graph between Cross sections and T_c for Cornell potential with Gaussian form of f (reverse processes).

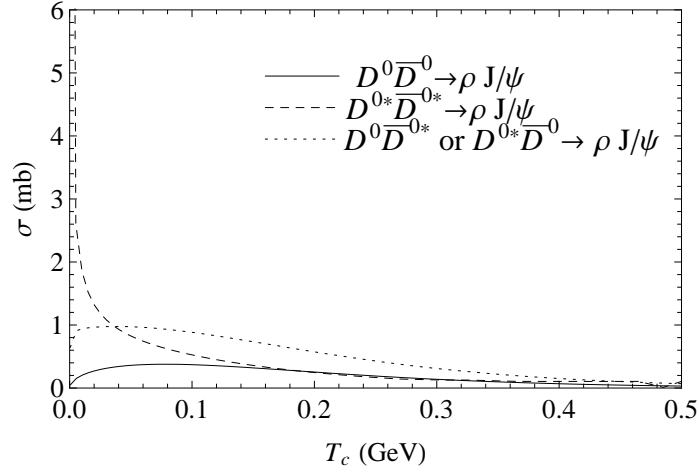


FIG. 9: Graph between Cross sections and T_c for Quadratic potential with Gaussian form of f (reverse processes).

- [22] A. M. Green, C. Michael and J. Paton, Phys. Lett. **B280**, 11 (1992).
- [23] Petrus Pennanen, Phys. Rev. **D55**, 3958 (1997).
- [24] A. M. Green, J. Koponen and P. Pennanen, Phys. Rev. **D61**, 014014 (1999).
- [25] Wayne. R. Thomas, Phys. Rev. **D41**, 3446 (1990).
- [26] M. Imran Jamil and Bilal Masud. Eur. Phys. Journal. **A47** 33 (2011).
- [27] Masud, B. Phys. Rev. **D50** 11 (1994).
- [28] M. Imran Jamil, Bilal Masud, Faisal Akram and S. M. Sohail Gilani, Chinese Physics **C41**, 013103 (2017).

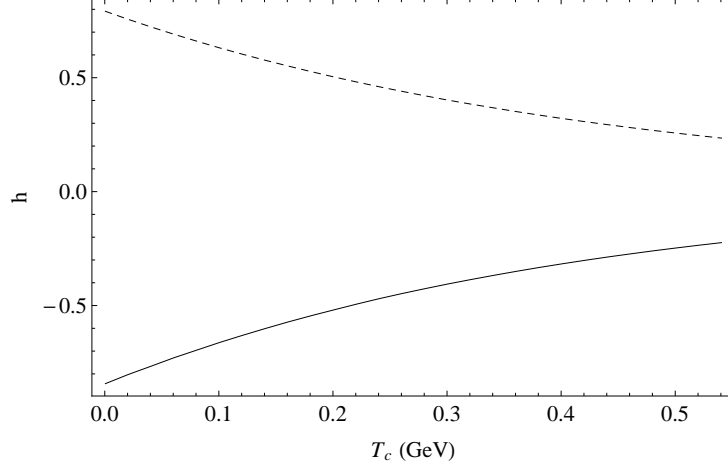


FIG. 10: Comparison of PE part and remaining terms of integratal equations with Cornell Potential after including f solid curve shows potential part.

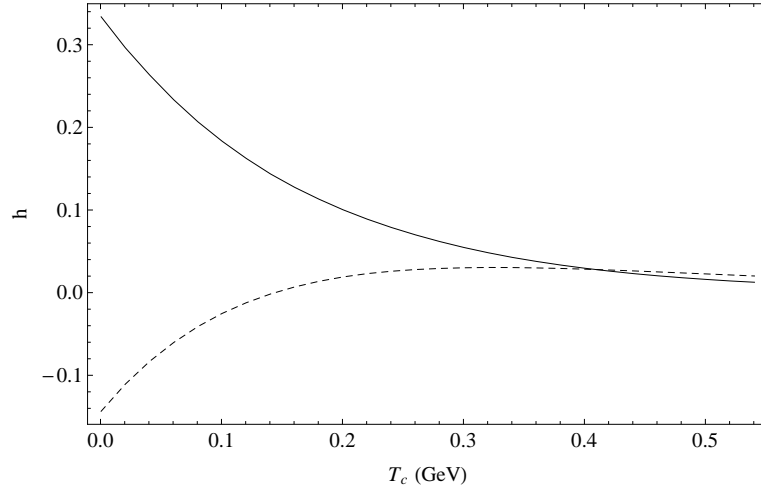


FIG. 11: Comparison of PE part and remaining terms of integral equations with Quadratic Potential after including f .

- [29] J. Burger, R. Muller, K. Tragl and H. M. Hofmann, Nuclear Physics. **A493**, 427 (1989).
- [30] Y. Suzuki and K. T. Hecht, Phys. Rev. **C27**, 299 (1983).
- [31] R. R. Schroder and H. G. Dosch, Nucl. Phys. **A451**: 666- 678 (1986).
- [32] Eduardo Cuervo-Reyes, Marcos Rigol and Jesus Rubayo-Soneirs, Rev.Bras.Ens.Fis.25:18 (2003).
- [33] Leonardo Galeta, Dan Porjol and Carlos Schat, 10.1103/PhysRev **D80** 116004 (2009).
- [34] Ding Xiaonan, Shin Pengnian, Zhang Zongye and Yu Youwen, Chinese Phys. Lett. **7**, 297

- (1988).
- [35] Jialun Ping, Chengrong Deng, Fan Wang, T. Goldman , Phys.Lett.**B659**:607-611 (2008).
 - [36] Zahra Ghalenovi, Francesco Giacosa and Dirk H. Rischke, Acta Phys.Polon. **B47** 1185 (2016).
 - [37] A. M. Green, J. Lukkarinen,t, P. Pennanen and C. Michael, Phys. Rev. **D53**, 1 (1996).
 - [38] Steven Weinberg, The Quantum Theory of Fields, Cambridge University Press, (1995).
 - [39] C. Patrnanani et al. (Particle Data Group), Chin. Phys. **C40**, 100001 (2016) .
 - [40] Nouredine Zettili, Quantum Mechanics, John Wiley and Sons, Ltd., (2001).
 - [41] Kevin L. Haglin and Charles Gale, Phys.Rev. **C63**, 065201 (2001).
 - [42] Ziwei Lin and C. M. Ko, Phys.Rev. **C62**, 034903 (2000).
 - [43] Yongseok Oh, Taesoo Song, and Su Houng Lee, Phys.Rev. **C63**, 034901 (2001).

Appendix A: The spin basis

For total spin 0 we have the following spin states

$$|P_{1\bar{3}}P_{2\bar{4}}\rangle_0 = \frac{1}{2}[\uparrow\uparrow\downarrow\downarrow - \uparrow\downarrow\downarrow\uparrow - \downarrow\uparrow\uparrow\downarrow + \downarrow\downarrow\uparrow\uparrow] \quad (\text{A1})$$

$$|V_{1\bar{4}}V_{2\bar{3}}\rangle_0 = \sqrt{\frac{1}{12}}[2\uparrow\downarrow\downarrow\uparrow + 2\downarrow\uparrow\uparrow\downarrow - \uparrow\uparrow\downarrow\downarrow - \uparrow\downarrow\uparrow\downarrow - \downarrow\uparrow\downarrow\uparrow - \downarrow\downarrow\uparrow\uparrow] \quad (\text{A2})$$

$$|V_{1\bar{3}}V_{2\bar{4}}\rangle_0 = \sqrt{\frac{1}{12}}[2\uparrow\downarrow\uparrow\downarrow + 2\downarrow\uparrow\downarrow\uparrow - \uparrow\uparrow\downarrow\downarrow - \uparrow\downarrow\downarrow\uparrow - \downarrow\uparrow\uparrow\downarrow - \downarrow\downarrow\uparrow\uparrow] \quad (\text{A3})$$

the spin overlaps are

$${}_0\langle P_{1\bar{3}}P_{2\bar{4}}|P_{1\bar{3}}P_{2\bar{4}}\rangle_0 = {}_0\langle V_{1\bar{3}}V_{2\bar{4}}|V_{1\bar{3}}V_{2\bar{4}}\rangle_0 = {}_0\langle V_{1\bar{4}}V_{2\bar{3}}|V_{1\bar{4}}V_{2\bar{3}}\rangle_0 = 1 \quad (\text{A4})$$

$${}_0\langle P_{1\bar{3}}P_{2\bar{4}}|V_{1\bar{4}}V_{2\bar{3}}\rangle_0 = {}_0\langle V_{1\bar{4}}V_{2\bar{3}}|P_{1\bar{3}}P_{2\bar{4}}\rangle_0 = \frac{-\sqrt{3}}{2} \quad (\text{A5})$$

$${}_0\langle V_{1\bar{3}}V_{2\bar{4}}|V_{1\bar{4}}V_{2\bar{3}}\rangle_0 = {}_0\langle V_{1\bar{4}}V_{2\bar{3}}|V_{1\bar{3}}V_{2\bar{4}}\rangle_0 = \frac{-1}{2} \quad (\text{A6})$$

By using the formalism $S_i.S_j = (\frac{\sigma_1}{2})_i(\frac{\sigma_1}{2})_j + (\frac{\sigma_2}{2})_i(\frac{\sigma_2}{2})_j + (\frac{\sigma_3}{2})_i(\frac{\sigma_3}{2})_j$ where $(\sigma_1)_i \uparrow_i = \downarrow_i$, $(\sigma_1)_i \downarrow_i = \uparrow_i$, $(\sigma_2)_i \uparrow_i = i \downarrow_i$, $(\sigma_2)_i \downarrow_i = -i \uparrow_i$, $(\sigma_3)_i \uparrow_i = \uparrow_i$, $(\sigma_3)_i \downarrow_i = -\downarrow_i$ ($i = 1, 2, \bar{3}, \bar{4}$), the matrix elements of $S_i.S_j$ in $|1\rangle_0$ and $|2\rangle_0$ basis were calculated to be

$${}_0\langle P_{1\bar{3}}P_{2\bar{4}}| \begin{pmatrix} S_1.S_2 \\ S_1.S_{\bar{3}} \\ S_1.S_{\bar{4}} \\ S_2.S_{\bar{3}} \\ S_2.S_{\bar{4}} \\ S_{\bar{3}}.S_{\bar{4}} \end{pmatrix} |P_{1\bar{3}}P_{2\bar{4}}\rangle_0 = \begin{pmatrix} 0 \\ -3/4 \\ 0 \\ 0 \\ -3/4 \\ 0 \end{pmatrix} \quad (\text{A7})$$

$${}_0\langle P_{1\bar{3}}P_{2\bar{4}}| \begin{pmatrix} S_1.S_2 \\ S_1.S_{\bar{3}} \\ S_1.S_{\bar{4}} \\ S_2.S_{\bar{3}} \\ S_2.S_{\bar{4}} \\ S_{\bar{3}}.S_{\bar{4}} \end{pmatrix} |V_{1\bar{4}}V_{2\bar{3}}\rangle_0 = {}_0\langle V_{1\bar{4}}V_{2\bar{3}}| \begin{pmatrix} S_1.S_2 \\ S_1.S_{\bar{3}} \\ S_1.S_{\bar{4}} \\ S_2.S_{\bar{3}} \\ S_2.S_{\bar{4}} \\ S_{\bar{3}}.S_{\bar{4}} \end{pmatrix} |P_{1\bar{3}}P_{2\bar{4}}\rangle_0 = \begin{pmatrix} \sqrt{3}/8 \\ 3\sqrt{3}/8 \\ -\sqrt{3}/8 \\ -\sqrt{3}/8 \\ 3\sqrt{3}/8 \\ \sqrt{3}/8 \end{pmatrix} \quad (\text{A8})$$

$${}_0\langle V_{1\bar{4}}V_{2\bar{3}}| \begin{pmatrix} S_1.S_2 \\ S_1.S_{\bar{3}} \\ S_1.S_{\bar{4}} \\ S_2.S_{\bar{3}} \\ S_2.S_{\bar{4}} \\ S_{\bar{3}}.S_{\bar{4}} \end{pmatrix} |V_{1\bar{4}}V_{2\bar{3}}\rangle_0 = \begin{pmatrix} -1/2 \\ -1/2 \\ 1/4 \\ 1/4 \\ -1/2 \\ -1/2 \end{pmatrix} \quad (\text{A9})$$

$${}_0\langle V_{1\bar{3}}V_{2\bar{4}}| \begin{pmatrix} S_1.S_2 \\ S_1.S_{\bar{3}} \\ S_1.S_{\bar{4}} \\ S_2.S_{\bar{3}} \\ S_2.S_{\bar{4}} \\ S_{\bar{3}}.S_{\bar{4}} \end{pmatrix} |V_{1\bar{3}}V_{2\bar{4}}\rangle_0 = \begin{pmatrix} -1/2 \\ 1/4 \\ -1/2 \\ -1/2 \\ 1/4 \\ -1/2 \end{pmatrix} \quad (\text{A10})$$

$${}_0\langle V_{1\bar{3}}V_{2\bar{4}}| \begin{pmatrix} S_1.S_2 \\ S_1.S_{\bar{3}} \\ S_1.S_{\bar{4}} \\ S_2.S_{\bar{3}} \\ S_2.S_{\bar{4}} \\ S_{\bar{3}}.S_{\bar{4}} \end{pmatrix} |V_{1\bar{4}}V_{2\bar{3}}\rangle_0 = {}_0\langle V_{1\bar{4}}V_{2\bar{3}}| \begin{pmatrix} S_1.S_2 \\ S_1.S_{\bar{3}} \\ S_1.S_{\bar{4}} \\ S_2.S_{\bar{3}} \\ S_2.S_{\bar{4}} \\ S_{\bar{3}}.S_{\bar{4}} \end{pmatrix} |V_{1\bar{3}}V_{2\bar{4}}\rangle_0 = \begin{pmatrix} 5/8 \\ -1/8 \\ -1/8 \\ -1/8 \\ -1/8 \\ 5/8 \end{pmatrix} \quad (\text{A11})$$

For total spin 1 we have following spin states

$$|P_{1\bar{3}}V_{2\bar{4}}\rangle_1 = \frac{1}{\sqrt{6}}[\uparrow\uparrow\downarrow\uparrow - \downarrow\uparrow\uparrow\uparrow + \frac{1}{\sqrt{2}}(\uparrow\uparrow\downarrow\downarrow + \uparrow\downarrow\downarrow\uparrow - \downarrow\uparrow\uparrow\downarrow - \downarrow\downarrow\uparrow\uparrow) + \uparrow\downarrow\downarrow\downarrow - \downarrow\downarrow\uparrow\downarrow] \quad (\text{A12})$$

$$|V_{1\bar{3}}V_{2\bar{4}}\rangle_1 = \frac{1}{\sqrt{12}}[\uparrow\uparrow\uparrow\downarrow + \uparrow\downarrow\uparrow\uparrow - \uparrow\uparrow\downarrow\uparrow - \downarrow\uparrow\uparrow\uparrow + \uparrow\downarrow\downarrow\downarrow + \downarrow\downarrow\uparrow\downarrow - \downarrow\uparrow\downarrow\downarrow - \downarrow\downarrow\uparrow\uparrow \\ + \sqrt{2}\uparrow\downarrow\uparrow\downarrow + \sqrt{2}\downarrow\uparrow\uparrow\downarrow] \quad (\text{A13})$$

$$|V_{1\bar{4}}V_{2\bar{3}}\rangle_1 = \frac{1}{\sqrt{12}}[\uparrow\uparrow\downarrow\uparrow + \uparrow\downarrow\uparrow\uparrow - \uparrow\uparrow\uparrow\downarrow - \downarrow\uparrow\uparrow\uparrow + \sqrt{2}\uparrow\downarrow\downarrow\uparrow - \sqrt{2}\downarrow\uparrow\uparrow\downarrow + \uparrow\downarrow\downarrow\downarrow \\ + \downarrow\downarrow\downarrow\uparrow - \downarrow\uparrow\downarrow\downarrow - \downarrow\downarrow\uparrow\downarrow] \quad (\text{A14})$$

the spin overlaps are

$${}_1\langle P_{1\bar{3}}V_{2\bar{4}}|P_{1\bar{3}}V_{2\bar{4}}\rangle_1 = {}_1\langle V_{1\bar{3}}V_{2\bar{4}}|V_{1\bar{3}}V_{2\bar{4}}\rangle_1 = {}_1\langle V_{1\bar{4}}V_{2\bar{3}}|V_{1\bar{4}}V_{2\bar{3}}\rangle_1 = 1 \quad (\text{A15})$$

$${}_1\langle P_{1\bar{3}}V_{2\bar{4}}|V_{1\bar{4}}V_{2\bar{3}}\rangle_1 = {}_1\langle V_{1\bar{4}}V_{2\bar{3}}|P_{1\bar{3}}V_{2\bar{4}}\rangle_1 = \frac{1}{\sqrt{2}} \quad (\text{A16})$$

$${}_1\langle V_{1\bar{3}}V_{2\bar{4}}|V_{1\bar{4}}V_{2\bar{3}}\rangle_1 = 0 \quad (\text{A17})$$

The matrix elements of $S_i.S_j$ in $|1\rangle_1$ and $|2\rangle_1$ basis were calculated to be

$${}_1\langle P_{1\bar{3}}V_{2\bar{4}}| \begin{pmatrix} S_1.S_2 \\ S_1.S_{\bar{3}} \\ S_1.S_{\bar{4}} \\ S_2.S_{\bar{3}} \\ S_2.S_{\bar{4}} \\ S_{\bar{3}}.S_{\bar{4}} \end{pmatrix} |P_{1\bar{3}}V_{2\bar{4}}\rangle_1 = \begin{pmatrix} 0 \\ -3/4 \\ 0 \\ 0 \\ 1/4 \\ 0 \end{pmatrix} \quad (\text{A18})$$

$${}_1\langle P_{1\bar{3}}V_{2\bar{4}}| \begin{pmatrix} S_1.S_2 \\ S_1.S_{\bar{3}} \\ S_1.S_{\bar{4}} \\ S_2.S_{\bar{3}} \\ S_2.S_{\bar{4}} \\ S_{\bar{3}}.S_{\bar{4}} \end{pmatrix} |V_{1\bar{4}}V_{2\bar{3}}\rangle_1 = {}_1\langle V_{1\bar{4}}V_{2\bar{3}}| \begin{pmatrix} S_1.S_2 \\ S_1.S_{\bar{3}} \\ S_1.S_{\bar{4}} \\ S_2.S_{\bar{3}} \\ S_2.S_{\bar{4}} \\ S_{\bar{3}}.S_{\bar{4}} \end{pmatrix} |P_{1\bar{3}}V_{2\bar{4}}\rangle_1 = \begin{pmatrix} -1/4\sqrt{2} \\ -3/4\sqrt{2} \\ 1/4\sqrt{2} \\ 1/4\sqrt{2} \\ 1/4\sqrt{2} \\ -1/4\sqrt{2} \end{pmatrix} \quad (\text{A19})$$

$${}_1\langle V_{1\bar{4}}V_{2\bar{3}}| \begin{pmatrix} S_1.S_2 \\ S_1.S_{\bar{3}} \\ S_1.S_{\bar{4}} \\ S_2.S_{\bar{3}} \\ S_2.S_{\bar{4}} \\ S_{\bar{3}}.S_{\bar{4}} \end{pmatrix} |V_{1\bar{4}}V_{2\bar{3}}\rangle_1 = \begin{pmatrix} -1/4 \\ -1/4 \\ 1/4 \\ 1/4 \\ -1/4 \\ -1/4 \end{pmatrix} \quad (\text{A20})$$

For total spin 2 we have following spin states

$$\begin{aligned} |V_{1\bar{3}}V_{2\bar{4}}\rangle_2 = |V_{1\bar{4}}V_{2\bar{3}}\rangle_2 = & \sqrt{\frac{1}{5}}[\downarrow\downarrow\downarrow\downarrow + \uparrow\uparrow\uparrow\uparrow + \frac{1}{2}(\downarrow\uparrow\downarrow\downarrow + \downarrow\downarrow\downarrow\uparrow + \uparrow\downarrow\downarrow\downarrow + \downarrow\downarrow\uparrow\downarrow + \uparrow\uparrow\uparrow\downarrow + \uparrow\downarrow\uparrow\uparrow \\ & + \uparrow\uparrow\downarrow\uparrow + \downarrow\uparrow\uparrow\uparrow) + \sqrt{\frac{1}{6}}(\uparrow\uparrow\downarrow\downarrow + \uparrow\downarrow\downarrow\uparrow + \downarrow\uparrow\uparrow\downarrow + \downarrow\downarrow\uparrow\uparrow + \downarrow\uparrow\downarrow\uparrow + \uparrow\downarrow\uparrow\downarrow)] \end{aligned} \quad (\text{A21})$$

the spin overlaps are

$${}_2\langle V_{1\bar{3}}V_{2\bar{4}}|V_{1\bar{4}}V_{2\bar{3}}\rangle_2 = {}_2\langle V_{1\bar{3}}V_{2\bar{4}}|V_{1\bar{3}}V_{2\bar{4}}\rangle_2 = {}_2\langle V_{1\bar{4}}V_{2\bar{3}}|V_{1\bar{4}}V_{2\bar{3}}\rangle_2 = 1 \quad (\text{A22})$$

The matrix elements of $S_i.S_j$ in $|1\rangle_2$ and $|2\rangle_2$ basis were calculated to be

$${}_2\langle V_{1\bar{3}}V_{2\bar{4}}|\begin{pmatrix} S_1.S_2 \\ S_1.S_{\bar{3}} \\ S_1.S_{\bar{4}} \\ S_2.S_{\bar{3}} \\ S_2.S_{\bar{4}} \\ S_{\bar{3}}.S_{\bar{4}} \end{pmatrix}|V_{1\bar{3}}V_{2\bar{4}}\rangle_2 = {}_2\langle V_{1\bar{4}}V_{2\bar{3}}|\begin{pmatrix} S_1.S_2 \\ S_1.S_{\bar{3}} \\ S_1.S_{\bar{4}} \\ S_2.S_{\bar{3}} \\ S_2.S_{\bar{4}} \\ S_{\bar{3}}.S_{\bar{4}} \end{pmatrix}|V_{1\bar{4}}V_{2\bar{3}}\rangle_2 = \begin{pmatrix} 1/4 \\ 1/4 \\ 1/4 \\ 1/4 \\ 1/4 \\ 1/4 \end{pmatrix} \quad (\text{A23})$$

$${}_2\langle V_{1\bar{3}}V_{2\bar{4}}|\begin{pmatrix} S_1.S_2 \\ S_1.S_{\bar{3}} \\ S_1.S_{\bar{4}} \\ S_2.S_{\bar{3}} \\ S_2.S_{\bar{4}} \\ S_{\bar{3}}.S_{\bar{4}} \end{pmatrix}|V_{1\bar{4}}V_{2\bar{3}}\rangle_2 = {}_2\langle V_{1\bar{4}}V_{2\bar{3}}|\begin{pmatrix} S_1.S_2 \\ S_1.S_{\bar{3}} \\ S_1.S_{\bar{4}} \\ S_2.S_{\bar{3}} \\ S_2.S_{\bar{4}} \\ S_{\bar{3}}.S_{\bar{4}} \end{pmatrix}|V_{1\bar{3}}V_{2\bar{4}}\rangle_2 = \begin{pmatrix} 1/4 \\ 1/4 \\ 1/4 \\ 1/4 \\ 1/4 \\ 1/4 \end{pmatrix} \quad (\text{A24})$$